



Universiteit
Leiden
The Netherlands

Photodynamic cancer therapy enhances accumulation of nanoparticles in tumor-associated myeloid cells

in't Veld, R.V.H.; Ritsma, L.; Kleinovink, J.W.; Que, I.; Ossendorp, F.; Cruz, L.J.

Citation

In't Veld, R. V. H., Ritsma, L., Kleinovink, J. W., Que, I., Ossendorp, F., & Cruz, L. J. (2020). Photodynamic cancer therapy enhances accumulation of nanoparticles in tumor-associated myeloid cells. *Journal Of Controlled Release*, 320, 19-31. doi:10.1016/j.jconrel.2019.12.052

Version: Publisher's Version

License: [Creative Commons CC BY 4.0 license](https://creativecommons.org/licenses/by/4.0/)

Downloaded from: <https://hdl.handle.net/1887/3181170>

Note: To cite this publication please use the final published version (if applicable).



Photodynamic cancer therapy enhances accumulation of nanoparticles in tumor-associated myeloid cells



Ruben V. Huis in 't Veld^a, Laila Ritsma^b, Jan Willem Kleinovink^c, Ivo Que^a, Ferry Ossendorp^d, Luis J. Cruz^{a,*}

^a Department of Radiology, Leiden University Medical Centre (LUMC), the Netherlands

^b Department of Cell and Chemical Biology, LUMC, Leiden, the Netherlands

^c Department of Medical Oncology, LUMC, Leiden, the Netherlands

^d Department of Immunohematology and Blood Transfusion, LUMC, Leiden, the Netherlands

ARTICLE INFO

Keywords:

Photodynamic therapy
Immunotherapy
Nanoparticles
PLGA
Cancer
Tumor microenvironment
Immune modulation
Theranostics
Pharmacology
Delivery

ABSTRACT

In cancer treatment, nanomedicines may be employed in an attempt to improve the tumor localization of antineoplastic drugs e.g. immunotherapeutic agents either through passive or active targeting, thereby potentially enhancing therapeutic effect and reducing undesired off-target effects. However, a large number of administered nanocarriers often fail to reach the tumor area. In the present study, we show that photodynamic therapy (PDT) enhances the tumor accumulation of systemically administered lipid-PEG layer coated poly (lactic-co-glycolic acid) (PLGA) nanoparticles (NP). Intravital microscopy and histological analysis of the tumor area reveal that the tumor vasculature was disrupted after PDT, disturbing blood flow and coinciding with entrapment of nanocarriers in the tumor area. We observed that the nanoparticles accumulating after treatment do not confine to specific locations within the tumor, but rather localize to various cells present throughout the tumor area. Finally, we show by flow cytometry that NP accumulation occurred mostly in immune cells of the myeloid lineage present in the tumor microenvironment (TME) as well as in tumor cells, albeit to a lower extent. These data expose opportunities for combination treatments of clinical PDT with NP-based immunotherapy to modulate the TME and improve antitumor immune responses.

1. Introduction

Photodynamic therapy (PDT) in cancer treatment is a minimally-invasive therapeutic modality that involves the administration of a light-absorbing photosensitizer (PS) and subsequent illumination with light, often of a specific wavelength in the red spectrum. It relies on the generation of reactive oxygen species that induce damage towards cells and structures within the illuminated area, resulting in a reduction of the tumor mass and potentially its surrounding vasculature. Bremachlorin is an established PS that has been approved for clinical applications in Russia under the brand name Radachlorin[®], that induces no reported side effects with the exception of mild to moderate pain during treatment in a subset of patients, has good tolerability and rapid excretion of the majority of the compound (98%) in human trials [1–3]. Due to absorption in the deep-red spectrum [4], the use of external light sources is suitable for superficial tumors. For more deeply seated tumors e.g. for colon cancer, fiber optics can be used to direct the light to

the tumor. Radachlorin[®]-PDT was found to be effective in the treatment of non-small cell lung cancer [2], basal cell carcinoma [1], endobronchial cancer [5], high grade bladder cancer [3] and early esophageal cancer [6], either as a standalone treatment or in combination settings. These studies have demonstrated the safety and potential of Radachlorin[®]-PDT in a clinical setting. However, they also underlined the necessity of improving therapeutic outcome to further enhance long-lasting responses and patient survival.

The importance and potential of combination treatments in enhancing the efficacy of antitumor therapy is increasingly appreciated [7–9]. In line with this, Radachlorin[®]-PDT was found to induce potent antitumor responses in combination with immunotherapy in preclinical models [10,11]. Upon administration, however, many antitumor agents often fail to localize to the tumor, inducing off-target effects that may result in undesired toxicities. Nanoparticles (NP) as carriers of antitumor therapeutics represent an attractive means of enabling combination treatment by enhancing the accumulation of their content in

* Corresponding author at: Group leader Translational Nanobiomaterials and Imaging, Department of Radiology, Room C2-187h, Leiden University Medical Centre (LUMC), Albinusdreef 2, 2333 ZA Leiden, the Netherlands.

E-mail address: l.j.cruz_ricondo@lumc.nl (L.J. Cruz).

<https://doi.org/10.1016/j.jconrel.2019.12.052>

Received 18 June 2019; Received in revised form 27 December 2019; Accepted 30 December 2019

Available online 31 December 2019

0168-3659/© 2020 The Authors. Published by Elsevier B.V. This is an open access article under the CC BY license (<http://creativecommons.org/licenses/by/4.0/>).

solid tumors [12]. This attractiveness is due to the flexibility of drug loading in such carrier systems that allows for various types of anti-tumor treatments in addition to the tunable physicochemical properties of NP-based systems that allow for specific enrichment of their content in the tumor area. Polymeric NP consisting of poly-lactic-co-glycolic acid (PLGA) represent an extensively studied type of NP-based drug carrier in cancer treatment [13]. An often-employed modification to improve the tumor accumulation of PLGA-NP is the addition of polyethylene glycol (PEG). This modification greatly enhances the circulation time through a reduction of clearance by the phagocytic system of the liver [13,14], thereby allowing the exploitation of the enhanced permeability and retention (EPR) effect [15]. In this way, the off-target delivery of compounds is reduced while the number of antineoplastic molecules in the tumor area increases, thereby improving the therapeutic index of the antitumor treatment.

Though PEGylated NP improve the therapeutic index of anticancer agents through the EPR, a large number of administrated NP still fail to reach the tumor [13]. Interestingly, low-fluence rate PDT has been reported to optimize the tumor localization of Doxil [16,17], a liposomal formulation of doxorubicin, possibly due to enhanced vessel permeability after PDT [18,19]. It has not yet been explored whether PDT at higher (≥ 100 mW/cm²) fluence rates, often employed in clinical PDT-protocols aiming for curative tumor ablation (in the case of clinically applied sensitizers e.g. Foscan® [20,21], Radachlorin® [1–3] and NPe6 [22,23]), results in the tumor accumulation of polymeric NP. In the present study, we show that PDT enhances the tumor accumulation of PLGA-PEG NP. In addition, we observed that the NP in the tumor area localize to tumor cells as well as other cell types. The vasculature was disrupted after treatment, hampering blood flow through the tumor as visualized by fluorescently labeled high molecular weight dextran. Furthermore, we show that the NP do not confine to certain areas within the tumor, but rather distribute to various cell types present throughout the tumor area. Finally, NP accumulation was most pronounced in immune cells of the myeloid compartment in the TME. These findings support a rationale for combination treatments of PDT with NP-based therapies, specifically treatments that induce antitumor immune responses through modulation of myeloid cell functions.

2. Materials and methods

2.1. Materials and reagents

PLGA (Resomer RG 502H, lactide:glycolide molar ratio 48:52 to 52:48) was purchased from Boehringer Ingelheim, Germany. Solvents used for PLGA preparation were obtained from Sigma-Aldrich (The Netherlands). The lipids were purchased from Avanti Polar Lipids (USA) and included 1,2-distearoyl-sn-glycero-3-phosphoethanolamine-N-[amine (polyethylene glycol)2000] (ammonium salt) and 1,2-distearoyl-sn-glycero-3-phosphoethanolamine-N-[methoxy(polyethylene glycol)-2000] (ammonium salt) (mPEG 2000 PE). Fluorescein-labeled 2,000,000 Da dextran (anionic, lysine fixable) was purchased from Thermofisher.

2.2. Preparation of PLGA-NP

PLGA NP with entrapped near-infrared fluorescence molecules were prepared using an o/w emulsion and solvent evaporation-extraction method [24–27]. In brief, 100 mg of PLGA was dissolved in 3 mL of dichloromethane (DCM) containing the near-infrared 700 (NIR700) (1,1'-diethyl-2, 2' dicarbocyanine iodide from Sigma Aldrich) dye (0.5 mg) or NIR800 (IR-780 iodide) dye (0.5 mg) and was added dropwise to 25 mL of aqueous 2% (w/v) PVA in distilled water before emulsification for 90 s using a sonicator (Branson, sonifier 250). The lipid mPEG 2000 PE (20 mg) was dissolved in DCM and added to the vial after which the DCM was removed by a stream of nitrogen gas. Subsequently, the emulsion was rapidly added to the vial containing the

lipids and the solution was homogenized for 30 s by sonification. Following overnight evaporation of the solvent at 4 °C, the PLGA NP were collected by centrifugation at 25000g for 10 min, washed four times with distilled water, and lyophilized.

2.3. Nanoparticle size and zeta-potential measurement

The average size of PLGA NP was measured by nanoparticle tracking analysis using a Nanosight (Malvern Panalytical). The zeta-potential of the particles was determined on a ZetaSizer Nano ZSP (Malvern Panalytical). For this purpose, PLGA NP were diluted to 1 mg/mL in water before measurement.

2.4. Determination of NIR700 and NIR800 contents inside PLGA NP

Entrapment efficiency of fluorescent NIR700 and NIR800 within PLGA were determined by digesting 10 mg NPs in 1 mL 0.8 mol/L NaOH overnight at 37 °C. The NIR fluorescence was measured at 700 nm and 800 nm relative to a standard curve using an Odyssey imaging system (Li-COR) (Table 1). For all the comparison experiments, all formulations were adjusted equivalently by the amount of dye.

2.5. Animals and tumor models

All animal experiments were carried out in line with the Code of Practice of the Dutch Animal Ethical Commission. Female C57BL/6 J mice of 6–12 weeks were purchased from Harlan Laboratories (ENVIGO, the Netherlands), and C57BL/6-albino mice were bred in the breeding facility of the Leiden University Medical Center (LUMC). All mice were housed under specified pathogen-free conditions in the animal facility of the LUMC. Murine Colon 38 (MC38) cells (kindly provided by Mario Colombo) were used for experiments without modification. For imaging and flow cytometry purposes, MC38 cells were lentivirally transduced with Cyan Fluorescent Protein (CFP) and sorted on a BD FACSAria II based on CFP⁺ to obtain MC38-CFP. All cells used were mycoplasma as well as MAP-tested before the start of experiments, cultured in IMDM medium (Lonza) supplemented with 8% Fetal Calf Serum (Greiner), 2 mM glutamin (Gibco), 100 IU/mL penicillin/streptomycin (Gibco) and 25 mM 2-mercaptoethanol (Sigma) and kept in an incubator (Panasonic) at 37 °C and 5% CO₂.

2.6. Uptake and binding of nanoparticles in tumor cells

MC38 cells were seeded in 96-well black plates (Greiner) at 5000 cells per well and allowed to attach overnight. Cells were then incubated at 37 °C (uptake) or 4 °C (binding) with 10 µg/mL PLGA-PEG-NIR700 or PLGA-PEG-NIR800. After a specified time, the cells were washed 3 times in PBS and fixed immediately with PBS containing 1% formalin (J.T. Baker) at 4 °C for 15 min. Cells were then washed in PBS and reconstituted in 100 µL PBS before measuring the fluorescence of NIR700 and NIR800 on a SpectraMax ID3 microplate reader (Molecular Devices).

2.7. Fluorescence microscopy of nanoparticles in tumor cells

MC38 cells were seeded in an 8-chamber polystyrene vessel tissue culture-treated glass slides (Corning) at 3000 cells per chamber and allowed to attach overnight. Cells were then incubated for 24 h with PLGA-PEG-NIR700 or PLGA-PEG-NIR800 at 10 µg/mL. After this time, the cells were washed 3 times in PBS and fixed in PBS containing 1% formalin (J.T. Baker) at 4 °C for 15 min. Cells were then washed in PBS and stained with 0.25 µM DAPI (Sigma), after which the chambers were removed. Coverslips were mounted on the glass slides using Mowiol mounting medium (Sigma-Aldrich) supplemented with 2.5% w/v DABCO (Merck) and sealed with nail polish. Slides were imaged on a Leica SP5 fluorescence microscope.

2.8. Toxicity of nanoparticles to MC38 cells

The toxicity of PLGA-PEG-NIR700 and PLGA-PEG-NIR800 to MC38 cells after 48 h and 72 h of incubation was determined by adding 3-(4,5-dimethylthiazol-2-yl)-5-(3-carboxymethoxyphenyl)-2-(4-sulfo-phenyl)-2H-tetrazolium (MTS) reagent (Abcam), and absorption was measured at 490 nm on a Bio-Rad iMark microplate absorbance reader after incubation.

2.9. Photosensitizer uptake and retention experiments

40,000 MC38 cells were plated in a 24-well plate (Corning) in culture medium and allowed to attach overnight at 37 °C and 5% CO₂ in an incubator (Panasonic). For the uptake experiments, cells were incubated with indicated concentrations of Radachlorin® (Radapharma International) for a specified time. Cells were then washed 3 times in PBS and fixed immediately for the uptake experiment before washing in PBS and fixing in PBS containing 1% formalin (J.T. Baker) at 4 °C for 15 min. Cells were then washed in PBS and reconstituted in FACS buffer (PBS with 0.5% BSA and 0.02% sodium azide) before analysis by flow cytometry on an LSR II (BD Biosciences). For the retention experiment, cells incubated with photosensitizer for 4 h were washed 3 times in PBS and supplied with fresh medium. After a specified amount of time, the cells were washed 3 times in PBS and fixed in PBS containing 1% formalin (J.T. Baker) at 4 °C for 15 min. Cells were then washed in PBS and reconstituted in FACS buffer before analysis by flow cytometry.

2.10. PDT in vitro assay

For PDT in vitro, 40,000 MC38 cells were plated in a 24-well plate (Corning) in culture medium and allowed to attach overnight at 37 °C and 5% CO₂ in an incubator (Panasonic). Cells were then incubated with Radachlorin® (Radapharma International) for a specified time, washed 3 times with PBS and supplied with fresh medium. Illumination was typically performed at a light intensity (fluence rate) of 100 mW/cm² for a total light dose (fluence) of 20 J/cm² using a 662 nm Milon Lakhta Laser, unless indicated otherwise. The next day, cells were stained with Annexin V-FITC (BD Pharmingen) at 3 µL per sample and 0.5 µM DAPI (Sigma) in annexin V binding buffer (0.1 M Hepes, 1.4 M NaCl, and 25 mM CaCl₂ in deionized water with a pH set to 7.4. sterile filtered using a 0.2 µm filter) before analysis by flow cytometry.

2.11. PDT tumor treatment and in vivo imaging

For PDT in vivo, mice were inoculated with 5 × 10⁵ MC38 tumor cells in 200 µL PBS on the left and/or right flanks as indicated. Mice were randomly divided into groups when tumors reached a size of approximately 125 mm³. A PDT protocol that is optimal for MC38 tumor treatment was performed as described earlier [10,11]. In brief, Radachlorin® was administered intravenously in the tail vein at 20 mg/kg and incubated at a drug-to-light interval of 6 h. The skin surrounding the tumor area was shaved right before illumination under isoflurane anesthesia at a fluence rate of 116 mW/cm² over 1000 s for a fluence of 116 J/cm². The next day, the mice were injected intravenously in the tail vein with 100 µL of 3 mg/mL PLGA-PEG-NIR700 or PLGA-PEG-NIR800 in PBS. Mouse conditions were checked regularly, and tumor sizes were measured three-weekly using a caliper. Fluorescence spectrometry imaging was performed using the IVIS Spectrum (Perkinelmer) under isoflurane anesthesia. Relevant areas were shaved right before measurement to minimize interference of the fluorescent signal. Measurements were performed at automatic exposure times at position C using filter settings relevant for NIR800.

2.12. Intravital imaging

Mice were inoculated with 5 × 10⁵ MC38-CFP tumor cells in 200 µL

PBS on the right flank and randomly divided into groups when tumors reached a size of approximately 360 mm³. Tumor-bearing mice were then treated with PDT as described. For measurements aiming to visualize the vasculature, mice were anesthetized by isoflurane the day after treatment in preparation of intravital imaging. A skin flap was induced by cutting around the tumor and carefully pulling away the skin with the tumor attached. Tumors were then suspended in PBS and a coverslip was placed between the tumor and microscope. Mice were then kept on a 37 °C heat pad and imaged on the ZEISS LSM 710 multiphoton microscope with Spectra-Physics and LASOS LDM-XT lasers. Vessels in the tumor area were identified by light microscopy and subsequently by second harmonic detection of collagen on the multiphoton microscope. 2 MDa-Dextran-FITC (Invitrogen) was administered intravenously into the tail vein during measurements. For NP detection in MC38-CFP tumors, mice were injected intravenously with 100 µL of 3 mg/mL PLGA-PEG-NIR700 in PBS the day after PDT. The day following NP administration, a skin flap was prepared for intravital imaging as described.

2.13. Ex vivo confocal microscopy

Mice were inoculated with 5 × 10⁵ MC38 tumor cells in 200 µL PBS on the right flank and randomly divided into groups when tumors reached a size of approximately 300 mm³. Tumor-bearing mice were treated with PDT as described and injected intravenously with PLGA-PEG-NIR700 the morning after treatment. Two days after administration of the mice were sacrificed, and tumors were excised for further analysis. Samples were fixed in a sodium phosphate buffer containing 1% formalin (J.T. Baker) and poly L-lysine (ThermoFisher) overnight at 4 °C. Samples were then washed, incubated in 30% sucrose (Sigma) at 4 °C for 6 h and frozen in Tissue-Tek O.C.T. (VWR) before cutting on a CryoStar NX70 cryostat (Thermo Scientific). Samples were collected on coverslips, rehydrated in PBS and permeabilized for 5 min with PBS containing 0.1% Triton X-100 (Sigma). Samples were then washed 3 × with PBS after which blocking was performed with PBA (PBS with 0.5% BSA and 0.02% sodium azide). Samples were then incubated overnight at 4 °C with primary antibody rat anti-mouse CD31 (Biolegend) or an antibody mix of rat anti-mouse CD45 (ThermoFisher) and rabbit anti-mouse Vimentin (Cell signaling) in PBA. After incubation, samples were washed 3 × in PBS before incubation with secondary antibodies goat anti-rat alexa fluor 488 (ThermoFisher) or an antibody mix of goat anti-rat alexa fluor 488 (ThermoFisher) and donkey anti-rabbit alexa fluor 555 (ThermoFisher) in PBA for 1 h at 20 °C. Coverslips were mounted with Vectashield DAPI (Vectorlabs) and analyzed on a Leica SP5 microscope after ≥6 h of hardening at room temperature. Data were analyzed using the processing package FIJI for the ImageJ software.

2.14. Analysis of nanoparticle accumulation in various cell subsets in the tumor area by flow cytometry

Mice were inoculated with 5 × 10⁵ MC38-CFP tumor cells in 200 µL PBS on the right flank and randomly divided into groups when tumors reached a size of approximately 300 mm³. Tumor-bearing mice were treated with PDT as described and injected intravenously with PLGA-PEG-NIR700 the morning after treatment. Two days after administration of NP the mice were sacrificed, and tumors were excised for further analysis. Tumors were equally divided into two parts of which half was used for ex vivo confocal microscopy and half for flow cytometry analysis. For flow cytometry, samples were then cut into small pieces and treated with Librase (Sigma) protease mix for 15–30 min at 37 °C. Single cell suspensions were obtained using a Falcon cell strainer (Corning) and samples were washed 2 × with 10 mL culture medium, counted and washed 2 × with FACS buffer (PBS with 0.5% BSA and 0.02% sodium azide). Samples were stained with antibody mixes for analysis by flow cytometry. All flow cytometric analyses were carried out on samples provided in FACS buffer on a BD LSR-II flow cytometer.

Panels consisted of antibodies CD11b-FITC (Biolegend), F4/80-PE (eBioscience), CD45.2-AF780 (eBioscience), Ly6G-R700 (Biolegend), Ly6C-BV605 (Biolegend) and 7AAD (Invitrogen) viability staining for the myeloid panel in addition to CD3e-FITC (eBioscience), CD49b-PE (BD Pharmingen), CD45.2-AF780 (eBioscience), CD8 α -R700 (BD Biosciences), CD4-BV605 (Biolegend) and 7AAD (Invitrogen) viability staining for the lymphoid panel.

2.15. Statistics

Graph Pad Prism software version 8 was used for statistical analysis. Data were analyzed as indicated for individual experiments.

3. Results

3.1. Design, preparation and characterization of PLGA NP

PLGA NP harboring either NIR700 nm dye, used for intravital microscopy, histology and analysis by flow cytometry due to optimal laser-filter combinations available, or NIR800 nm dye, used for in vivo imaging due to optimal spectral imaging options available, were produced using the biodegradable polymer PLGA. The PLGA NP surface was coated with a polyethylene glycol (PEG)-lipid layer to minimize non-specific binding and to improve the blood circulation time. Fig. 1A schematically displays the resulting PLGA NP, PLGA-PEG-NIR700 and PLGA-PEG-NIR800, used for in vivo imaging and summarizes their physicochemical properties (Supplementary Table 1). PLGA-PEG-NIR700 displayed an average size of $\sim 133.4 \pm 41.2$ nm in diameter and a zeta potential of -14.4 mV, whereas the PLGA-PEG-NIR800 was found to have an average size of $\sim 144.7 \pm 42.7$ nm in diameter and a zeta potential of -19.1 mV (Fig. 1B & C). Moreover, the fluorescence of the NIR700 nm or NIR800 nm dye per mg particle was determined by IVIS fluorescence spectrometry (Fig. 1D), showing strong signal at the appropriate wavelengths in both NP. The NP were visualized by fluorescence microscopy (Fig. 1E), showing presence in the cytoplasm and are taken up by MC38 tumor cells over time when incubated at 37°C , but not at 4°C , indicating active uptake (Fig. 1F). Finally, the NP display no toxicity to MC38 cells up to a concentration of $200 \mu\text{g}/\text{mL}$ after 48 h and 72 h of incubation (Fig. 1G). These data show that PLGA-PEG-NIR700 and PLGA-PEG-NIR800 are non-toxic NP with a uniform size and negative zeta potential that are suitable for in vivo imaging after systemic administration.

3.2. Radachlorin[®] characterization and PDT in vitro

The uptake of Radachlorin[®] in tumor cells was determined by incubating MC38 cells with various concentrations of the photosensitizer (PS) before fixation and detection by flow cytometry. The uptake revealed strong fluorescence in MC38 cells increasing up to 4 h after incubation at concentrations ranging from 1 to $100 \mu\text{M}$, while incubation with $0.1 \mu\text{M}$ induced barely detectable uptake (Fig. 2A). The retention of Radachlorin[®] in MC38 cells after 4 h incubation was followed over time and revealed retention of the PS up to at least 6 h at similar levels to 0 h after the pulse (Fig. 2B). Based on these data, the dark toxicity of Radachlorin[®] towards MC38 cells was determined after 4 h of incubation at indicated concentrations. Viability of the cells was detected by flow cytometry following overnight incubation, staining with Annexin-V-FITC for early apoptotic cells and DAPI for dead cells. This revealed no PS toxicity in MC38 cells at concentrations of 0.1 – $10 \mu\text{M}$ and very low toxicity at a concentration of $100 \mu\text{M}$ (Fig. 2C). For PDT in vitro, MC38 cells were incubated for 4 h with various concentrations of PS and illuminated with 662 nm light at a light intensity (fluence rate) of $100 \text{ mW}/\text{cm}^2$ for a total light dose (fluence) of $20 \text{ J}/\text{cm}^2$. This protocol induced $> 99\%$ Annexin V⁺/DAPI⁺ cells after overnight incubation at concentrations of 1 – $100 \mu\text{M}$ (Fig. 2D). The fluence required for tumor cell toxicity in vitro was determined by incubation of MC38 with $1 \mu\text{M}$

PS for 4 h and PDT at $100 \text{ mW}/\text{cm}^2$, revealing $> 99\%$ Annexin V⁺/DAPI⁺ cells total light doses of 10 – $20 \text{ J}/\text{cm}^2$ (Fig. 2E). Finally, the fluence rate required for tumor cell toxicity in vitro was determined by incubation of MC38 with $1 \mu\text{M}$ PS for 4 h and PDT for $20 \text{ J}/\text{cm}^2$, showing $> 99\%$ Annexin V⁺/DAPI⁺ cells after overnight incubation at 25 – $200 \text{ mW}/\text{cm}^2$ (Fig. 2F). These data show that Radachlorin[®] is easily taken up by MC38 cells and retained for extended periods of time. In addition, the PS displays no dark toxicity to MC38 cells up to high concentrations and induces complete cell death after PDT at PS concentrations ranging from 1 to $100 \mu\text{M}$, light intensities of 25 – $200 \text{ mW}/\text{cm}^2$ and total light doses of 10 – $20 \text{ J}/\text{cm}^2$.

3.3. Photodynamic therapy enhances nanoparticle accumulation in tumors

To test whether PDT has an effect on the tumor accumulation of polymeric NP, PDT was performed on C57BL/6 albino mice bearing a single MC38 tumor of $\sim 125 \text{ mm}^3$ as described previously [10,11]. In brief, illumination of the tumor area with 662 nm light at $116 \text{ mW}/\text{cm}^2$ for $116 \text{ J}/\text{cm}^2$ over 1000 s was initiated 6 h after intravenous administration of Radachlorin[®] (Fig. 3A). The next morning, $100 \mu\text{L}$ of $3 \text{ mg}/\text{mL}$ PLGA-PEG-NIR800 in PBS was administered intravenously after which the NIR800 fluorescence was followed over time by in vivo fluorescence spectrometry. The treatment induced strong MC38 tumor regression (Fig. 3B) without inducing weight loss as an indication of treatment-induced toxicity (Fig. 3C), indicating successful therapy as reported previously [10]. The NIR800 fluorescence in PDT treated tumors was strongly increased compared to tumors in control mice starting from 24 h and up to 144 h after treatment (Fig. 3D & E). These results indicate that PDT enhances the tumor accumulation of PLGA-PEG-NIR800 nanoparticles in the first days after treatment.

3.4. PDT enhances specific nanoparticle accumulation in treated tumors without altering accumulation in untreated tumors

We next investigated whether PDT would also enhance the accumulation of NP in mice bearing multiple tumors. Treatment of primary tumors with Radachlorin[®]-PDT has been shown to induce a CD8⁺ T cell-related effect on distant, untreated, tumors [11]. As an inflammatory immune response is known to induce vasodilation and enhance vascular permeability, we investigated whether PDT will also affect NP accumulation in distant, untreated, tumors. To test this, C57BL/6 albino mice bearing two MC38 tumors were treated with PDT as described for only one tumor (PDT-treated mice) or were left untreated (control mice). All mice were injected intravenously with PLGA-PEG-NIR800 in PBS the morning after the treatment was performed (Fig. 4A). Again, PDT induced strong MC38 tumor regression on treated tumors without inducing body weight loss, while untreated tumors showed progressive growth (Fig. 4B&C). The NIR800 fluorescence signal in the PDT-treated tumors was strongly enhanced versus all untreated tumors at 24 h up to 144 h after administration of the NP (Fig. 4D & E). The NIR800 signal in the treated tumors was also enhanced when compared to untreated tumors of PDT-treated mice only (Supplementary Fig. 1A). There was no difference in fluorescence signal in untreated tumors of PDT-treated and control mice (Supplementary Fig. 1B), showing that PDT does not alter the accumulation of NP in untreated tumors. These data show that PDT enhances NP accumulation in treated tumors in a two-tumor model, without affecting the accumulation of NP in untreated tumors.

3.5. Intravital imaging reveals a disrupted tumor vasculature after PDT treatment

The previous results show that PDT enhances the NP accumulation to the tumor area after intravenous injection. As Radachlorin[®] has been described to be present in the vasculature at 6 h after intravenous administration [28], we hypothesized that the vasculature may be altered

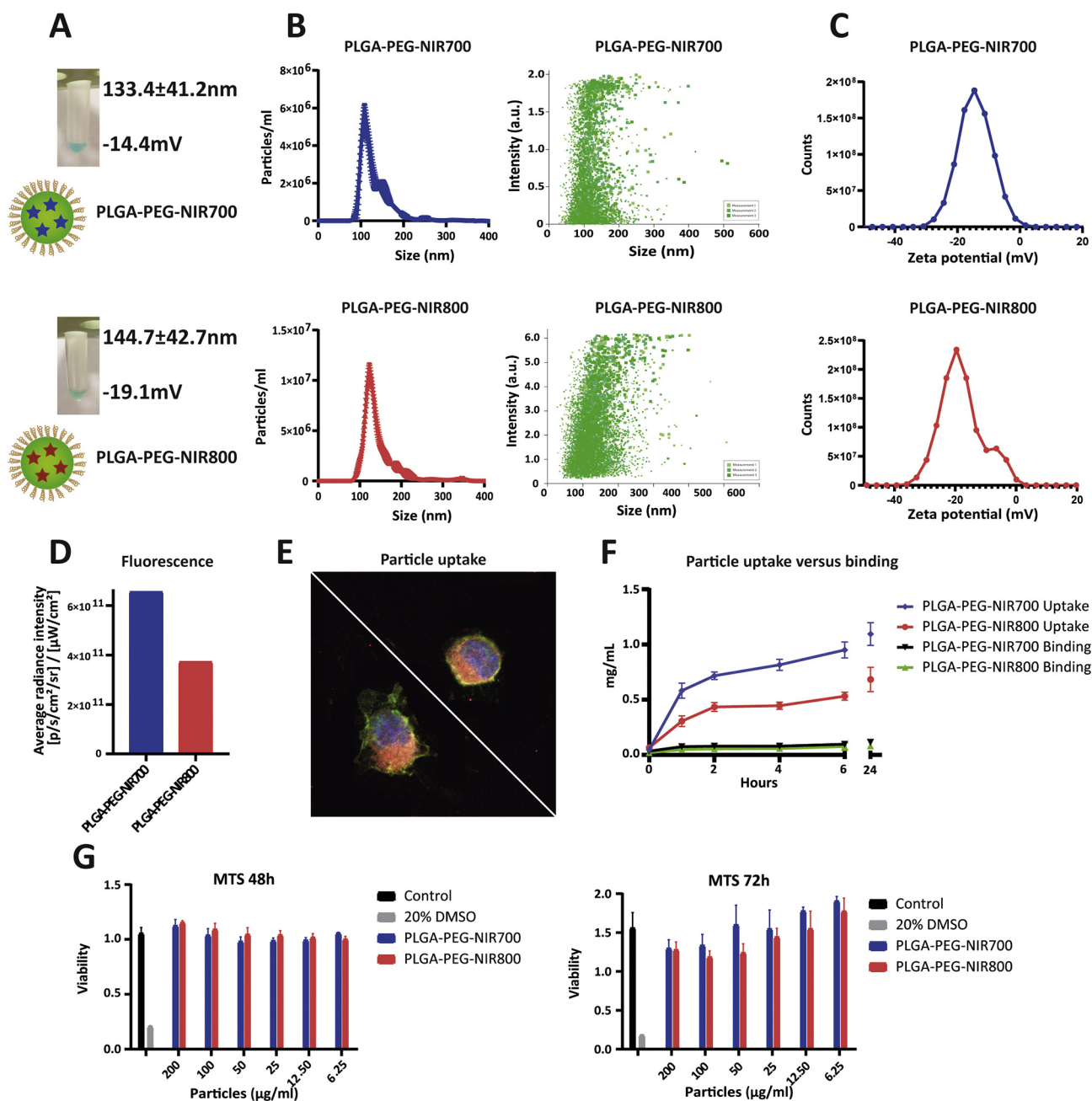


Fig. 1. Design, preparation and characterization of PLGA NP.

A) Schematic representation of PLGA-PEG-NIR700, used for histology and analysis by flow cytometry due to optimal laser-filter combinations available, and PLGA-PEG-NIR800, used for in vivo imaging due to optimal spectral imaging options available, in addition to a photograph displaying the NP in solution and a summary of their physicochemical characteristics. B) Size distribution in nm \pm SD and C) zeta potential of PLGA-PEG-NIR700 and PLGA-PEG-NIR800 determined by nanoparticle tracking analysis using a Nanosight. D) The fluorescence intensity of the encapsulated dye in PLGA-PEG-NIR700 and PLGA-PEG-NIR800 per mg particle, measured by IVIS fluorospectrometry. E) Fluorescence microscopy images of NP in MC38 tumor cells after 24 h of incubation with 10 μ g/mL of NIR700. F) Uptake versus binding of NP in MC38 cells over time, measured using the SpectraMax ID3 platereader G) Toxicity of PLGA-PEG-NIR700 and PLGA-PEG-NIR800 towards MC38 cells after 48 h and 72 h of incubation at indicated concentration, detected by MTS assay.

after treatment, thereby contributing to the enhanced NP administration. To seek whether the vasculature was visibly affected after PDT treatment, we performed in vivo imaging of the tumor area. We inoculated albino C57BL/6 J with MC38 cells lentivirally transduced with Histone 2B Cyan Fluorescent Protein (MC38-CFP) that stably expresses CFP fluorescence in the nucleus of transduced cells, to allow visualization of MC38 tumor cells on the ZEISS LSM 710 multiphoton microscope (Fig. 5A). Flow cytometric analysis shows that > 92% of MC38-CFP cells were CFP⁺ (Supplementary Fig. 2). When the tumors reached an average size of \sim 360 mm³, we performed PDT as described.

PDT induced MC38 tumor regressions on treated tumors (Fig. 5B) without inducing weight loss (Fig. 5C), indicating successful treatment despite large tumor sizes at the start of treatment. The day after treatment, a skin flap and an injection setup were prepared, enabling intravenous administration of 2 MDA-Dextran-FITC in the tail vein during tumor imaging. In untreated mice, the vasculature in the tumors displayed strong 2 MDA-dextran-FITC signal, showing intact vessels, and could not be observed the tumor area (Fig. 5D left panel). However, there were no intact vessels stained by 2 MDA-dextran-FITC in the tumor area of PDT-treated mice (Fig. 5D, right panel), and 2 MDA-

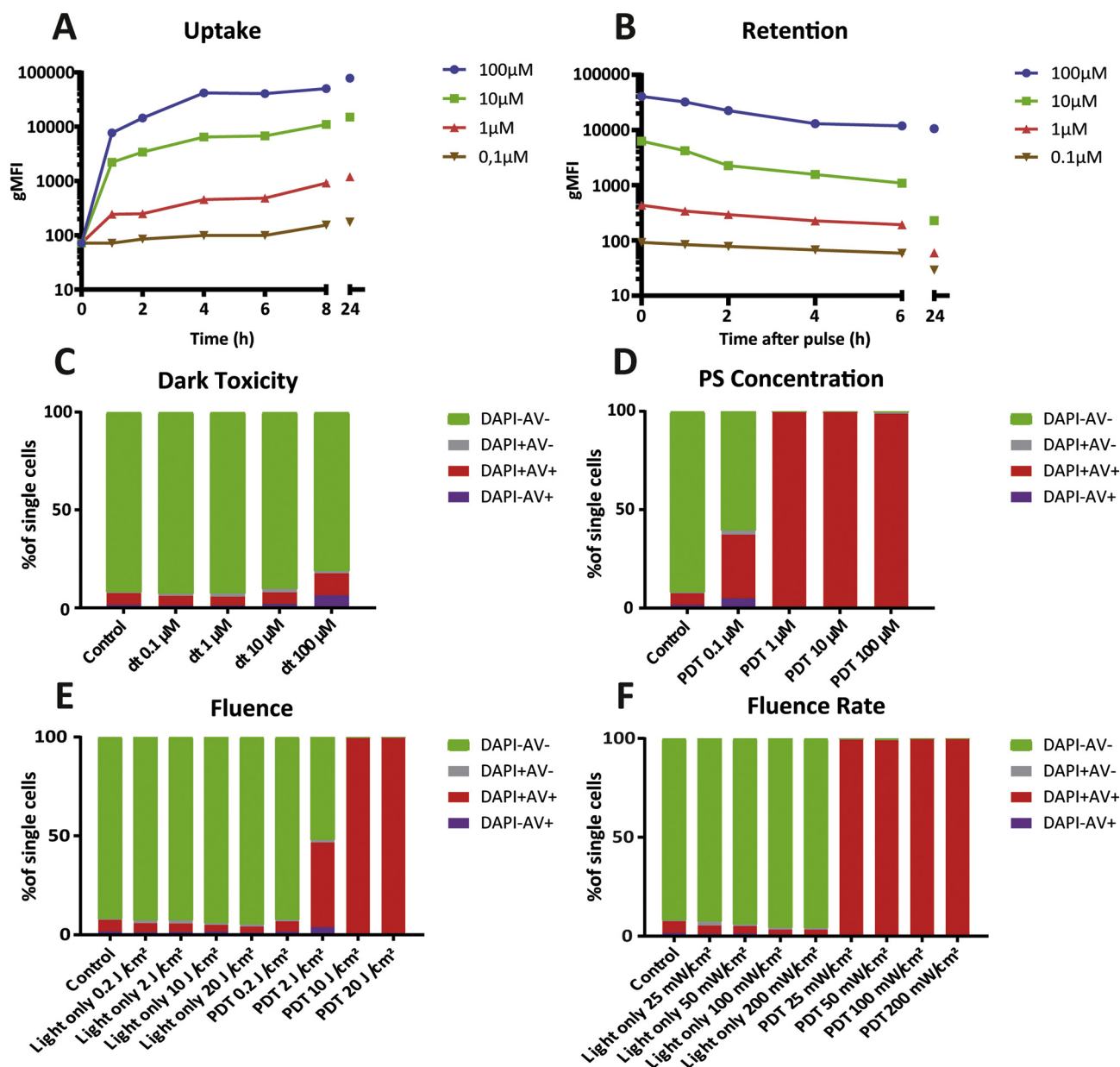


Fig. 2. Radachlorin[®] uptake, retention and PDT in vitro.

A) Uptake of Radachlorin[®] at indicated concentrations in MC38 cells over time and B) retention of Radachlorin[®] in MC38 after 4 h incubation over time. Cells were fixed in 1% formalin before detection by flow cytometry. C) Dark toxicity of Radachlorin[®] in MC38 cells after staining with early apoptosis marker Annexin V (AV⁺) and dead cell marker (DAPI⁺), measured by flow cytometry. The effect of D) PS concentration, E) fluence and F) fluence rate on the in vitro cytotoxicity of Radachlorin[®]-PDT on MC38 cells, determined by flow cytometry after staining with Annexin V and DAPI.

dextran-FITC was again not observed in the tumor area. As a control, vessels outside of the tumor area in the same PDT-treated animals were visualized and displayed strong FITC signal, indicating successful administration of Dextran (Fig. 5D middle panel) and suggesting that Radachlorin[®]-PDT disrupts the tumor vasculature.

To further investigate the tumor vasculature after treatment, we performed PDT on established MC38 tumor-bearing mice as described. Three days after PDT treatment, the mice were sacrificed for histological analysis (Fig. 6A). Samples were stained for DAPI and CD31, as a marker for endothelial cells, and show intact vessel structures in control mice. However, PDT treated tumors show a disrupted vasculature staining, displayed as a disperse staining pattern. Quantification of the CD31 staining was performed, showing a strong reduction in the percentage CD31⁺ pixels for PDT versus control tumors. Together, these data show that PDT disrupts the vasculature in the tumor area in a

manner that prevents intratumoral visualization of 2 MDa-Dextran-FITC.

3.6. NP localize to various cell types present throughout the tumor area

To investigate the localization of the NP in the tumor after PDT treatment, we administered PLGA-PEG-NIR700 the day after PDT treatment in the protocol depicted in Fig. 5A. At 24 h after NP administration, a skin flap was prepared to allow intravital imaging. In control mice, most NP (red signal) appear to be in close proximity to the nuclear CFP signal (Supplementary Fig. 3A), indicating their association with tumor cells. In PDT-treated mice, the NP localize near as well as far from the nuclear CFP signal (Supplementary Fig. 3B), indicating that the NP are partially associated with tumor cells but are also present outside of areas occupied by tumor cells.

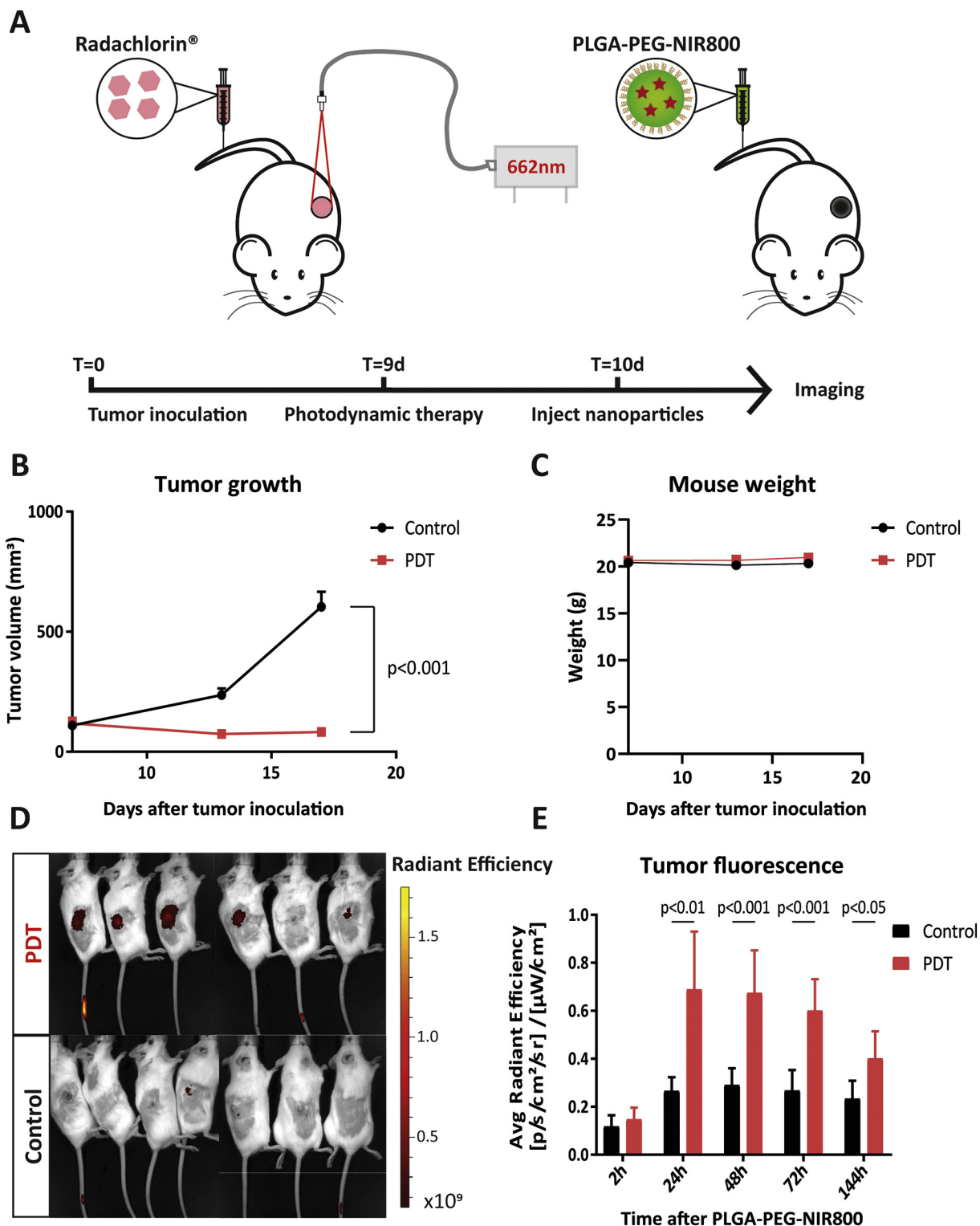


Fig. 3. PDT enhances NP accumulation in mice bearing a single tumor.

A) Schematic of the protocol: mice were inoculated subcutaneously with 0.5×10^6 MC38 cells in 200 μ L PBS on the right flank. At day 7, when the tumors were an average size of ~ 125 mm³, Radachlorin®-PDT was performed by illumination of the tumor area with 662 nm light at 116 mW/cm² for 116 J/cm² over 1000 s. The day after treatment, 100 μ L of a 3 mg/mL of PLGA-PEG-NIR800 was injected intravenously in the tail vein after which the fluorescence in the tumors was measured on the IVIS fluorospectrometer over time. B) Tumor growth curves and C) weight of PDT-treated and control mice, displayed as the mean + SEM for each group. D) Representative image of the NIR800 fluorescence in the tumor area in PDT-treated (upper panels) and control mice (lower panels) at 48 h after administration of the NP. Minimum fluorescence values were set to 1.50×10^8 and maximum fluorescence values were set to 1.75×10^9 across all images, to allow visual comparison E) Fluorescence intensity of the NIR800 signal in the tumors of PDT-treated and control mice over time, obtained using the IVIS fluorescence spectrometer. Statistical significance was determined using (multiple) Student's *t*-tests at various timepoints ($n = 7$ animals per group, * $p < .05$, ** $p < .01$ and *** $p < .001$).

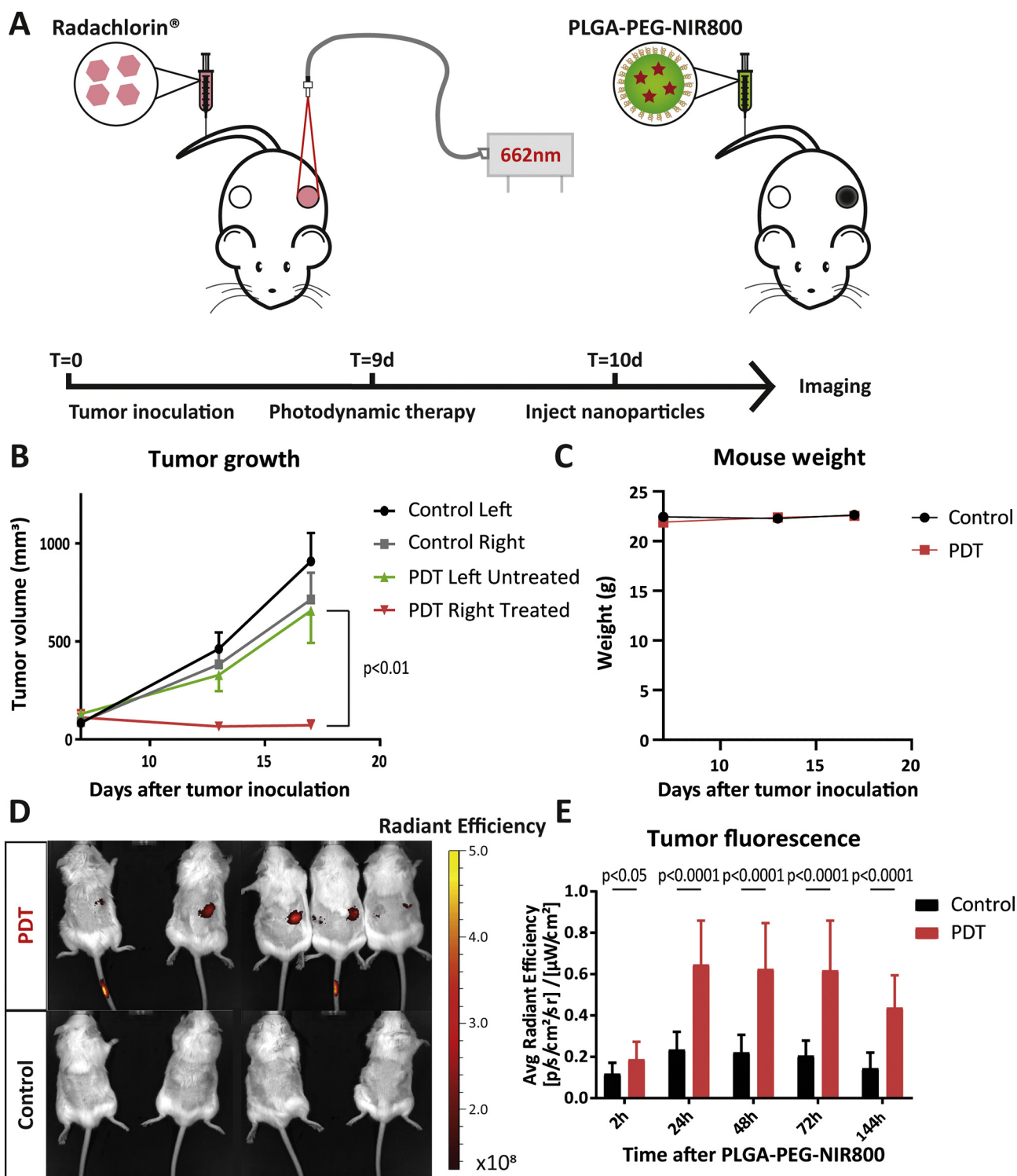


Fig. 4. PDT enhances NP accumulation in mice bearing double tumors.

A) Schematic of the protocol: mice were inoculated subcutaneously with 0.5×10^6 MC38 cells in 200 μ L PBS on the left and right flank. At day 7, when the tumors were an average size of ~ 125 mm³, Radachlorin®-PDT was performed by illumination of the tumor on the right flank with 662 nm light at 116 mW/cm² for 116 J/cm² over 1000 s. The day after treatment, 100 μ L of a 3 mg/mL of PLGA-PEG-NIR800 was injected intravenously in the tail vein after which the fluorescence in all tumors was measured on the IVIS fluorospectrometer over time. B) Tumor growth curves and C) weight of the PDT-treated and control tumors in treated mice as well as untreated tumors in control mice, displayed as the mean + SEM for each group. D) Representative image of the NIR800 fluorescence in the tumor area in PDT-treated (upper panels) with PDT treated tumors on the right flank, untreated tumors on the left flank and control mice (lower panels) at 48 h after NP administration. Minimum fluorescence values were set to 1.3×10^8 and maximum fluorescence values were set to 5.0×10^8 across all images, to allow visual comparison E) Fluorescence intensity of the NIR800 signal in PDT-treated versus all control tumors in treated as well as untreated mice over time, obtained using the IVIS fluorescence spectrometer. Statistical significance was determined using (multiple) Student's *t*-tests at various timepoints ($n = 7$ animals per group, * $p < .05$, ** $p < .01$, *** $p < .001$ and **** $p < .0001$).

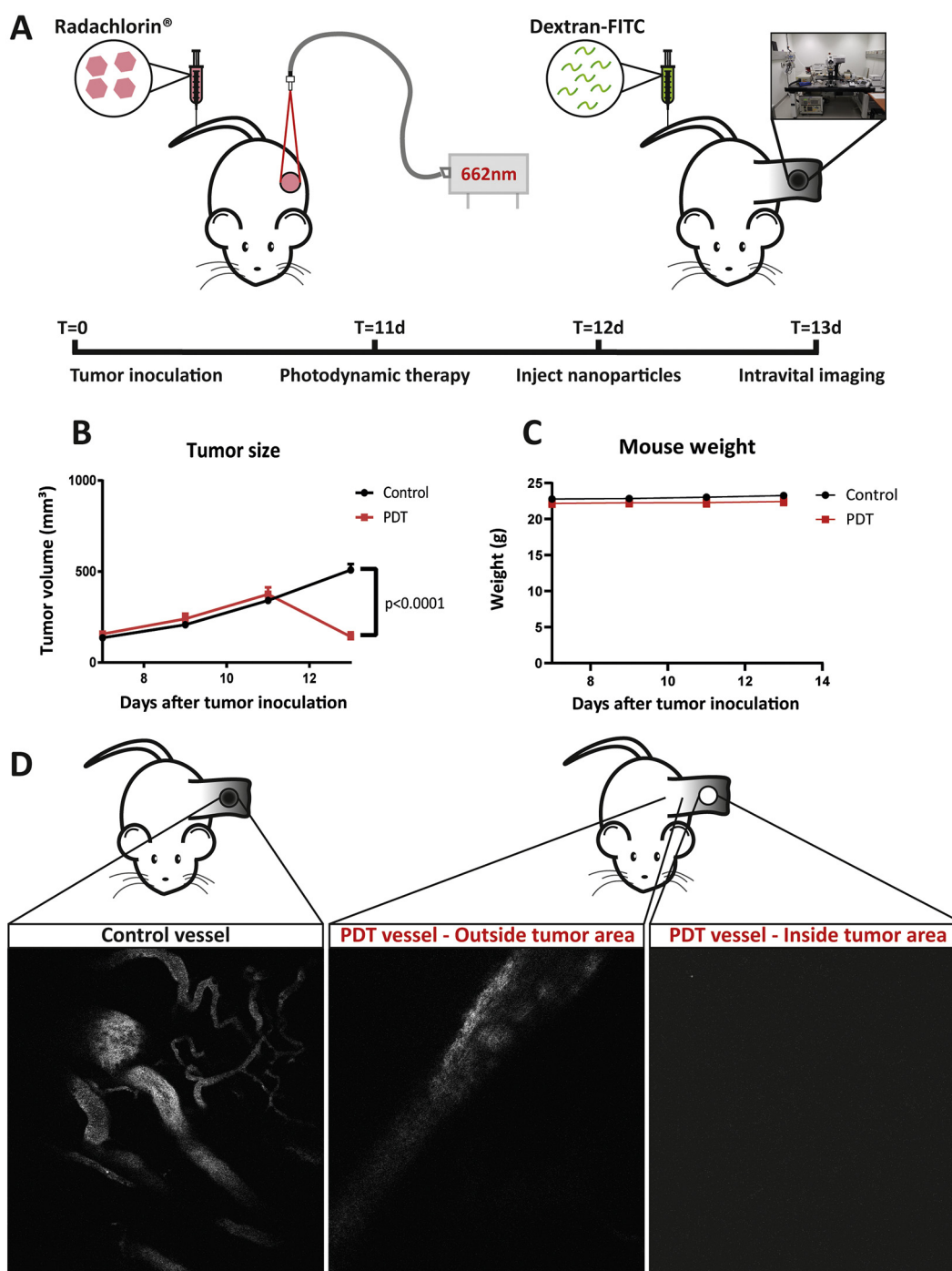


Fig. 5. Intravital imaging reveals a disrupted tumor vasculature after PDT treatment.

A) Schematic of the protocol: mice were inoculated subcutaneously with 0.5×10^6 MC38-CFP cells in 200 μ L PBS on the right flank. At day 11, when the tumors displayed an average size of ~ 360 mm³, Radachlorin®-PDT was performed by illumination of the tumor on the right flank with 662 nm light at 116 mW/cm² for 116 J/cm² over 1000 s. The day after treatment, a skin flap was prepared to allow intravital imaging and 2 M-dextran-FITC was injected during imaging for visualization of the vasculature. B) Tumor growth curves and C) weight of the PDT-treated and control tumors in treated mice as well as untreated tumors in control mice, displayed as the mean + SEM for each group. D) Representative visualization of the 2 Mda-dextran-FITC fluorescence signal present in the vasculature of control (left panel) and PDT-treated mice outside (middle panel) as well as inside (right panel) the tumor area ($n = 4$ animals per group).

To further investigate the localization of the NP in the tumor after treatment, we treated MC38 tumor-bearing mice with PDT as depicted in Fig. 6A. The day after treatment, PLGA-PEG-NIR700 was injected intravenously into the tail vein. Two days after administration of the NP, when the NP fluorescence intensity was previously determined to be elevated (Fig. 1D), the mice were sacrificed for analysis by histology. Samples were stained for DAPI, CD45 (immune cells) and vimentin

(mesenchymal cells). NIR700 fluorescence is observed throughout the tumor area and localizes close to CD45⁺ and vimentin⁺ cells in addition to cells staining negative for both markers (Fig. 6C). Furthermore, quantification of the fluorescence intensity shows an enhanced NIR700 fluorescence signal for PDT versus control tumors. To test for autofluorescence induced by the treatment, a histological analysis of NIR700 fluorescence in the tumor area of PDT treated tumors was

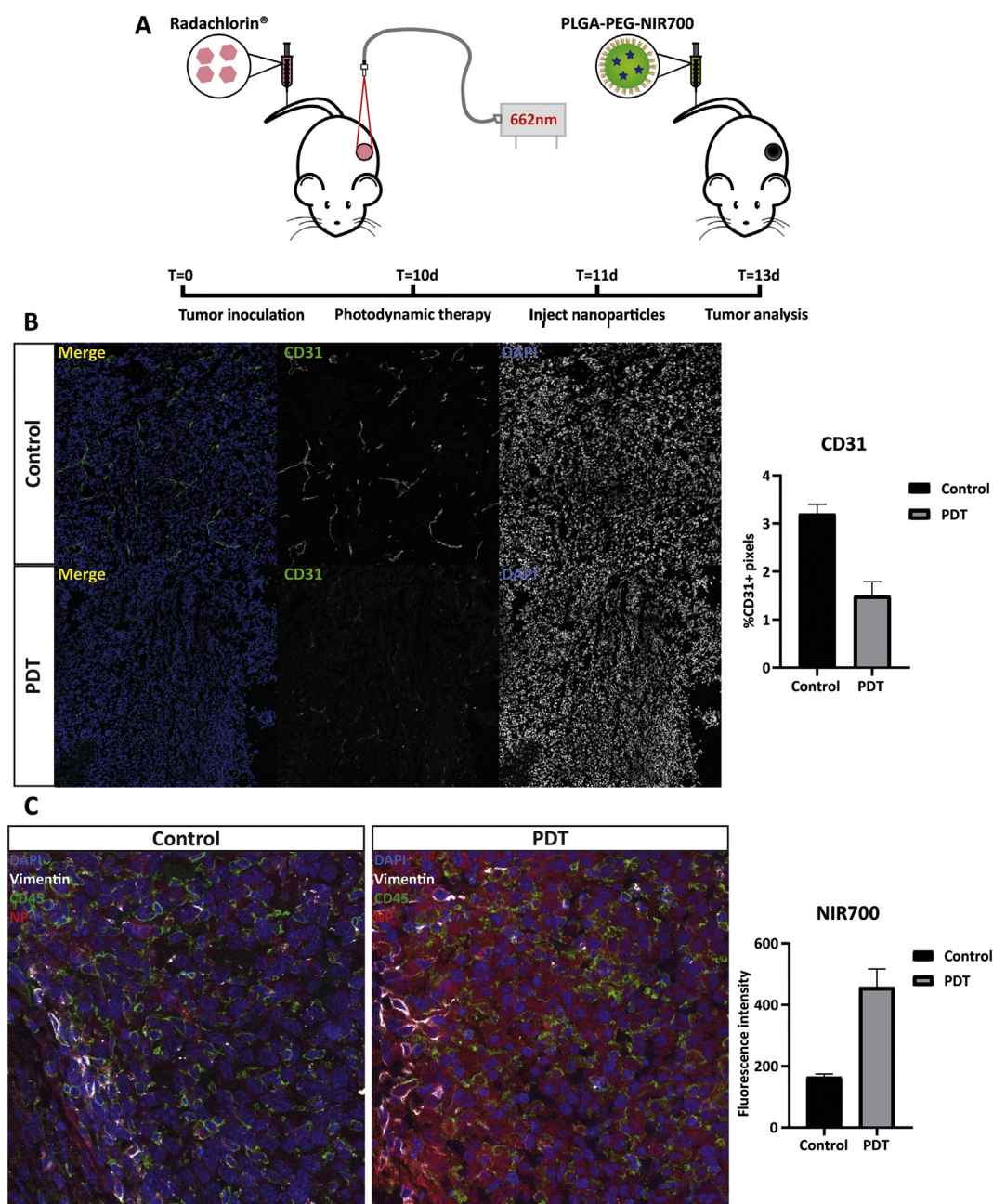


Fig. 6. Histological analysis of the tumor vasculature after PDT and PLGA-PEG-NIR700 fluorescence in the tumor area.

A) Schematic of the protocol: mice were inoculated subcutaneously with 0.5×10^6 MC38 cells in 200 μ L PBS on the right flank. At day 10, when the tumors displayed an average size of $\sim 300 \text{ mm}^3$, Radachlorin®-PDT was performed by illumination of the tumor on the right flank with 662 nm light at 116 mW/cm^2 for 116 J/cm^2 over 1000 s. The day after treatment, 100 μ L of a 3 mg/mL of PLGA-PEG-NIR700 NP was injected intravenously in the tail vein and incubated for 48 h. Mice were then sacrificed and tumors were excised for histology. B) Representative images of control (upper panels) as well as PDT (lower panels) samples stained for CD31 (green in Merge) and DAPI (blue in Merge) and analysis of the percentage of CD31⁺ pixels in PDT versus control samples ($n = 4$ animals per group). C) Representative images of the NIR700 signal (red) in control (left panel) as well as PDT (right panel) samples stained for DAPI (blue), CD45 (green) and Vimentin (white) and analysis of the fluorescence intensity of NIR700 in PDT versus control samples ($n = 4$ animals per group).

performed in absence of administered NP and showed background signal when compared to PDT treated tumors where NP were administered (supplementary Fig. 4). These results indicate that NP distributing towards the tumor localize to multiple types of cells throughout the tumor area, rather than confining to specific tumor sites.

3.7. NP are primarily taken up by cells of the myeloid compartment in the tumor microenvironment

To determine whether the NP localize to specific cellular subsets in the TME, we performed flow cytometry on MC38-CFP tumor-bearing mice treated as in Fig. 6A. Gating strategies were employed to allow evaluation of the myeloid and lymphoid cell compartments of the immune cell infiltrates and all data shown were gated to contain only viable, single cell populations (Supplementary Fig. 5). PDT induced a significant reduction in the total amount CD45⁺ cells (Fig. 7A) as well

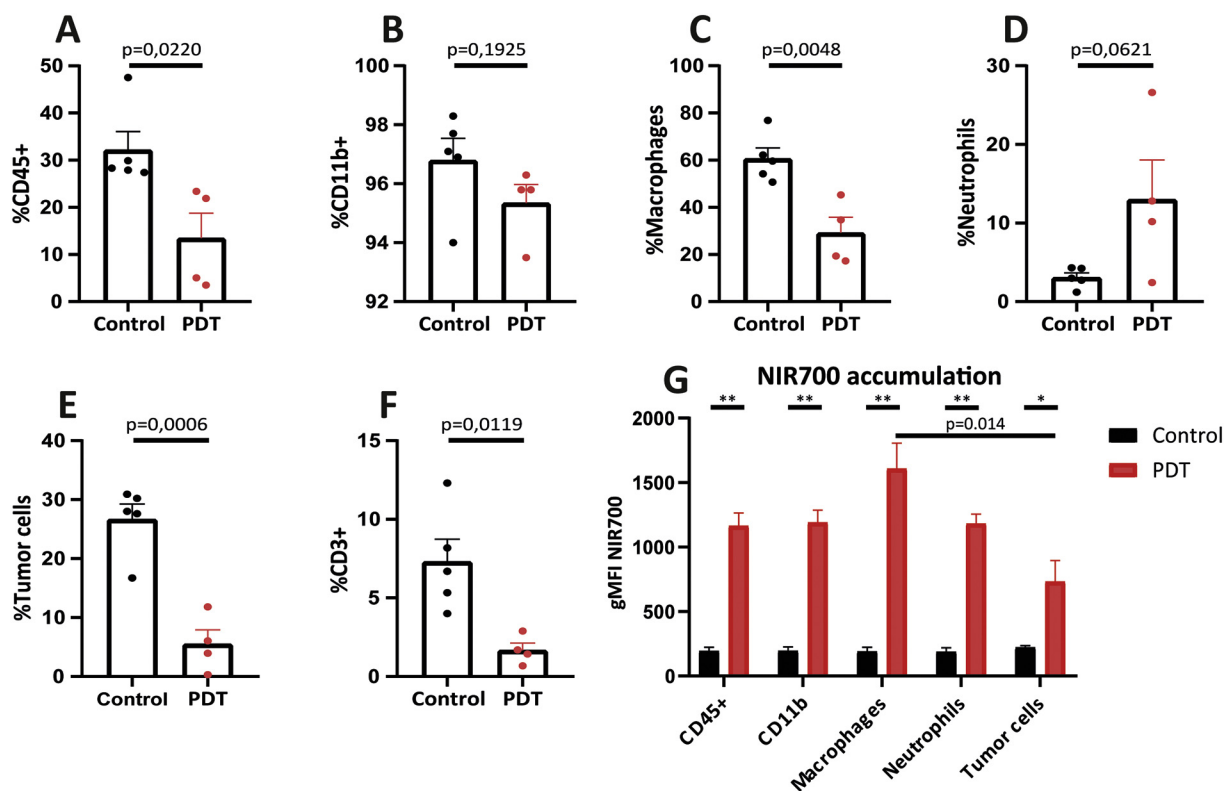


Fig. 7. NP in the tumor area accumulate strongly in cells of the myeloid compartment. Mice were inoculated subcutaneously with 0.5×10^6 MC38-CFP cells in 200 μ L PBS on the right flank and treated as depicted in Figure 6A. At day 10, when the tumors displayed an average size of ~ 300 mm³, Radachlorin®-PDT was performed by illumination of the tumor on the right flank with 662 nm light at 116 mW/cm² for 116 J/cm² over 1000 s. The day after treatment, 100 μ L of a 3 mg/mL of PLGA-PEG-NIR700 NP was injected intravenously in the tail vein and incubated for 48 h. Mice were then sacrificed and tumors were excised for analysis of the cellular composition of the TME by flow cytometry. A-F) Representation of cellular subsets present in the tumors of PDT-treated and control mice. CD45⁺ are shown as a percentage of live cells (DAPI⁻ within the single cell gate). CD11b⁺ are defined as CD45⁺CD11b⁺ and shown as a percentage of CD45⁺ (DAPI⁻ within the single cell gate), macrophages are defined as CD45⁺CD11b⁺ F4/80⁺ and shown as a percentage of CD45⁺, neutrophils are defined as CD45⁺CD11b⁺Ly6G⁺ and shown as a percentage of CD45⁺, tumor cells are defined as CFP⁺CD45⁻ and shown as a percentage of live cells, and CD3⁺ are defined as CD45⁺CD3⁺ and shown as a percentage of CD45⁺. G) geometric mean fluorescence intensity (gMFI) of NIR700 in PDT-treated versus control tumors for various subsets. Statistical significance was determined using a two-tailed Student's *t*-test between groups ($n = 5$ control and $n = 4$ PDT animals, * $p < .01$, ** $p < .001$).

as a non-significant reduction in the amount of CD11b⁺ cells as a percentage of CD45⁺ cells (Fig. 7B) in the tumor. The percentages of macrophages, shown as a percentage of CD45⁺ cells, were also significantly reduced after PDT (Fig. 7C), while the percentages of neutrophils as a percentage of CD45⁺ were increased (Fig. 7D). This is in line with the literature, where infiltrating immune cells at early time-points after treatment were reported to mainly consist of neutrophils [29]. The amount of viable tumor cells was also significantly reduced after treatment (Fig. 7E). Furthermore, the percentage of CD3⁺ cells as a percentage of CD45⁺ were very strongly reduced (Fig. 7F), indicating that PDT strongly diminishes the amount of T cells present in the tumor at early time points after treatment. Moreover, the numbers of CD3⁺ cells in the PDT group were too low for an accurate analysis of NP accumulation in this subset. In all subsets, the amount of NIR700 signal was markedly increased in PDT treated versus control mice (Fig. 7G). The increase was most pronounced in the macrophage subset, with a relative increase of up to approximately 10 \times . Uptake of NIR700 in tumor cells was also increased after PDT, albeit to a lesser extent than in the subsets of myeloid origin, as indicated by statistical significance in fluorescence in macrophages versus tumor cells of PDT treated mice (Fig. 7G).

These data reveal that PDT greatly enhances the accumulation of NP in cells of the myeloid compartment throughout the tumor area. As the benefits of combination treatments are becoming more apparent [7–9], the development of therapeutic protocols whereby PDT is performed in an optimal setting to achieve strong antitumor efficacy that can be

combined with other types of antitumor treatments to enhance therapeutic outcome. Our data suggest a strong potential synergy for combinations of PDT and NP-based immunotherapy that benefit from enhanced uptake by cells of the myeloid lineage.

Mice were inoculated subcutaneously with 0.5×10^6 MC38-CFP cells in 200 μ L PBS on the right flank and treated as depicted in Fig. 6A. At day 10, when the tumors displayed an average size of ~ 300 mm³, Radachlorin®-PDT was performed by illumination of the tumor on the right flank with 662 nm light at 116 mW/cm² for 116 J/cm² over 1000 s. The day after treatment, 100 μ L of a 3 mg/mL of PLGA-PEG-NIR700 NP was injected intravenously in the tail vein and incubated for 48 h. Mice were then sacrificed and tumors were excised for analysis of the cellular composition of the TME by flow cytometry. A-F) Representation of cellular subsets present in the tumors of PDT-treated and control mice. CD45⁺ are shown as a percentage of live cells (DAPI⁻ within the single cell gate). CD11b⁺ are defined as CD45⁺CD11b⁺ and shown as a percentage of CD45⁺ (DAPI⁻ within the single cell gate), macrophages are defined as CD45⁺CD11b⁺ F4/80⁺ and shown as a percentage of CD45⁺, neutrophils are defined as CD45⁺CD11b⁺Ly6G⁺ and shown as a percentage of CD45⁺, tumor cells are defined as CFP⁺CD45⁻ and shown as a percentage of live cells, and CD3⁺ are defined as CD45⁺CD3⁺ and shown as a percentage of CD45⁺. G) geometric mean fluorescence intensity (gMFI) of NIR700 in PDT-treated versus control tumors for various subsets. Statistical significance was determined using a two-tailed Student's *t*-test between groups ($n = 5$ control and $n = 4$ PDT animals, * $p < .01$, ** $p < .001$).

4. Discussion

For the administration of many antitumor drugs, a delicate balance between off target toxicities and therapeutic efficacy must be maintained. Therefore, increasing the distribution of such drugs to tumors on a per administration basis may help to improve therapeutic outcome. In the present study, we show that PDT enhances the tumor distribution of a single dose of PEGylated NP based on PLGA, a carrier of antitumor drugs that has been investigated extensively [30,31]. It was shown previously that low-fluence rate PDT enhances the tumor localization of liposomal doxorubicin (Doxil)^{16,17,18,19}. We show here that PDT at relatively high fluence rates, often employed in PDT protocols in the clinic, also enhances the tumor distribution of PLGA-PEG NP. Furthermore, we show that PDT enhances NP accumulation in treated tumors of mice bearing two tumors on opposite flanks. We have previously reported that PDT on primary tumors inhibits the tumor growth of distant, untreated tumors in a T cell dependent manner [11]. We show here that this effect does not alter the NP distribution to those untreated tumors.

In addition, we show that PDT disrupts the tumor vasculature in a way that prevents 2 MDa-dextran-FITC to visualize the tumors while the tumor-surrounding vasculature remained intact, allowing visualization by 2 MDa dextran-FITC. Histological analysis revealed a severely disrupted CD31 staining pattern and a reduction in the percentage of CD31+ pixels in PDT treated tumors. Moreover, NP were found to distribute throughout the tumor and associate with several cell types present in the tumor area. These results indicate that NP are able to localize to PDT treated tumors though the intact vessels surrounding the vasculature, where they can easily enter the tumor through the disrupted vasculature. As the blood flow in PDT treated tumors is hampered, this may prevent the NP from leaving, thereby essentially trapping them in the tumor area. In contrast to the NP, the 2 MDa dextran-FITC could not be observed in the tumor area outside of the vasculature in control as well as treated mice. This may either be due to the 2 MDa dextran-FITC diluting in the tumor area to an extent that falls below the detection limit of the current setup, or the inability of the relatively large branched polymer to leak out of the vessels in control mice in addition to their inability to leak out of the disrupted vessels and/or move through tumor area in treated mice. Together, these data strengthen observations that PDT can enhance carrier-based antitumor therapy by increasing the number of encapsulated agents that benefit from raising the concentration of active molecules, e.g. doxorubicin in Doxil, in the tumor area.

Finally, we show that PDT enhances the NP content in all several cellular subsets present in the tumor. NP uptake can be facilitated through phagocytosis, macropinocytosis as well as caveolae-, clathrin-, and scavenger receptor-mediated endocytic pathways, depending on the properties of the NP [32]. Cells that facilitate phagocytosis and are therefore likely to phagocytose NP include macrophages, DCs, monocytes and neutrophils. Moreover, macrophages, and neutrophils to a lesser extent, are described to facilitate most of the NP uptake, processing and clearance of nanomaterials in organs such as the liver, spleen and kidneys [33,34]. In line with this, we show that NP uptake in the tumor is most pronounced in the macrophage population, where the NP content was significantly increased versus tumor cells in PDT treated tumors. PDT has been described to induce antitumor immune responses that at early time points after treatment consist mainly of infiltrating myeloid cells [35–37]. Administration of NP the day following treatment may therefore ensure that many of the administered NP localize to those cell types. In conclusion, the protocol presented here describes a strong PDT-mediated antitumor efficacy while inducing vascular disruption and ensuring NP accumulation in the tumor area. The observation that the NP accumulating in the tumor area preferentially localize to cells of the myeloid origin provide a strong rationale for combinations of PDT with NP-based immunotherapy that exerts its effects on immune cells of myeloid origin. Examples of such

immunotherapies include the use of myeloid depleting or modulating agents, immune stimulants e.g. toll-like receptor (TLR)-ligands, cytokines and stimulator of interferon genes (STING) agonists to invoke or enhance antitumor immune responses.

Author contributions

L.J. Cruz and F. Ossendorp designed and supervised the study. Huis in 't Veld R.V wrote the manuscript and performed the main experiments. L.J. Cruz and Huis in 't Veld R.V assembled the nanoparticles. Que. I. and Kleinovink E.J.W. supported the animal studies. Ritsma L., performed the intravital imaging.

Funding sources

This work is part of the research program 723.012.110 (Vidi, L.J. Cruz) and 016.176.081 (Veni, L. Ritsma), which is financed by the Dutch Organization for Scientific Research (NWO). Also, we would like to thank the financial support of the LUMC fellowship grant (L.J. Cruz) and an LUMC Gisela Thier Fellowship grant, a subsidy from the Leids Universiteits Fonds (LUF, CWB 7204, L. Ritsma), the New Chemical Innovation grant 731.015.206 (L.J. Cruz), project grants from the EU Program H2020-MSCA-2015-RISE (644373– PRISAR, L.J. Cruz), MSCA-ITN-2015-ETN (675742-ISPIC, L.J. Cruz), H2020-MSCA-ITN-ETN (675743-ISPIC, L.J. Cruz), H2020-MSCA-2016-RISE (734684-CHARMED, L.J. Cruz) and H2020-MSCA-RISE-2017-CANCER (777,682, L.J. Cruz).

Declaration of Competing Interest

The authors were supported with funding from Leiden University Medical Center and the Netherlands Organization for Scientific Research (NWO). The authors have no other relevant affiliations or financial involvement with any organization or entity with a financial interest in, or financial conflict with, the subject matter or materials discussed in the manuscript, apart from those already disclosed.

Acknowledgements

D.L. Marvin kindly performed the transduction of MC38 to obtain the MC38-CFP cell line.

Appendix A. Supplementary data

Supplementary data to this article can be found online at <https://doi.org/10.1016/j.jconrel.2019.12.052>.

References

- [1] E.V. Kochneva, E.V. Filonenko, E.G. Vakulovskaya, E.G. Scherbakova, O.V. Seliverstov, N.A. Markichev, A.V. Reshetnikov, Photosensitizer Radachlorin®: skin Cancer PDT phase II clinical trials, *Photodiagn. Photodyn. Ther.* 7 (2010) 258–267.
- [2] W. Ji, J. wan Yoo, E.K. Bae, J.H. Lee, C.M. Choi, The effect of Radachlorin® PDT in advanced NSCLC: a pilot study, *Photodiagn. Photodyn. Ther.* 10 (2013) 120–126.
- [3] J.Y. Lee, R.R. Diaz, K.S. Cho, M.S. Lim, J.S. Chung, W.T. Kim, W.S. Ham, Y.D. Choi, Efficacy and safety of photodynamic therapy for recurrent, high grade nonmuscle invasive bladder cancer refractory or intolerant to Bacille Calmette-Guérin immunotherapy, *J. Urol.* 190 (2013) 1192–1199.
- [4] A.B. Uzdensky, O.Y. Dergacheva, A.A. Zhavoronkova, A.V. Reshetnikov, G.V. Ponomarev, Photodynamic effect of novel Chlorin E6 derivatives on a single nerve cell, *Life Sci.* 74 (2004) 2185–2197.
- [5] A. Akopov, A. Rusanov, A. Gerasin, N. Kazakov, M. Urtenova, I. Chistyakov, Preoperative Endobronchial photodynamic therapy improves Resectability in initially Irresectable (inoperable) locally advanced non small cell lung Cancer, *Photodiagn. Photodyn. Ther.* 11 (2014) 259–264.
- [6] E.V. Filonenko, V.V. Sokolov, V.I. Chissov, E.A. Lukyanets, G.N. Vorozhtsov, Photodynamic therapy of early Esophageal cancer, *Photodiagn. Photodyn. Ther.* 5 (2008) 187–190.
- [7] J.S. Lopez, U. Banerji, Combine and conquer: challenges for targeted therapy combinations in early phase trials, *Nat. Rev. Clin. Oncol.* 14 (2017) 57–66.

- [8] K.M. Mahoney, P.D. Rennett, G.J. Freeman, Combination cancer immunotherapy and new immunomodulatory targets, *Nat. Rev. Drug Discov.* 14 (2015) 561–584.
- [9] P. Gotwals, S. Cameron, D. Cipolletta, V. Cremasco, A. Crystal, B. Hewes, B. Mueller, S. Quarantino, C. Sabatos-Peyton, L. Petruzzelli, et al., Prospects for combining targeted and conventional Cancer therapy with immunotherapy, *Nat. Rev. Cancer* 17 (2017) 286–301.
- [10] J.W. Kleinovink, P.B. van Driel, T.J.A. Snoeks, N. Prokopi, M.F. Fransen, L. Javier Cruz, L. Mezzanotte, A. Chan, C.W.G.M. Lowik, F. Ossendorp, Combination of photodynamic therapy and specific immunotherapy efficiently eradicates established tumors, *Clin. Cancer Res.* 22 (6) (2016) 1459–1468.
- [11] J.W. Kleinovink, M.F. Fransen, C.W. Löwik, F. Ossendorp, Photodynamic-immune checkpoint therapy eradicates local and distant Tumors by CD8(+) T cells, *Cancer Immunol. Res.* 5 (2017) 832–838.
- [12] C.G. Da Silva, F. Rueda, C.W. Löwik, F. Ossendorp, L.J. Cruz, Combinatorial prospects of Nano-targeted chemoimmunotherapy, *Biomaterials* 83 (2016) 308–320.
- [13] S. Rezvantab, N.I. Drude, M.K. Moraveji, N. Güvener, E.K. Koons, Y. Shi, T. Lammers, F. Kiessling, PLGA-based nanoparticles in cancer treatment, *Front. Pharmacol.* 9 (2018) 1260.
- [14] A. Grigoletto, A. Mero, I. Zanusso, O. Schiavon, G. Pasut, Chemical and enzymatic site specific PEGylation of HGH: the stability and in vivo activity of PEG-*N*-terminal-HGH and PEG-Gln141-HGH conjugates, *Macromol. Biosci.* 16 (2016) 50–56.
- [15] H. Maeda, J. Wu, T. Sawa, Y. Matsumura, K. Hori, Tumor Vascular permeability and the EPR effect in macromolecular therapeutics: a review, *J. Control. Release* 65 (2000) 271–284.
- [16] J.W. Snyder, W.R. Greco, D.A. Bellnier, L. Vaughan, B.W. Henderson, Photodynamic therapy: a means to enhanced drug delivery to tumors, *Cancer Res.* 63 (2003) 8126–8131.
- [17] W. Gao, Z. Wang, L. Lv, D. Yin, D. Chen, Z. Han, Y. Ma, M. Zhang, M. Yang, Y. Gu, Photodynamic therapy induced enhancement of Tumor vasculature permeability using an Upconversion Nanoconstruct for improved Intratumoral nanoparticle delivery in deep tissues, *Theranostics* 6 (2016) 1131–1144.
- [18] B. Chen, B.W. Pogue, J.M. Luna, R.L. Hardman, P.J. Hoopes, H.T. Tumor Vascular, Permeabilization by Vascular-targeting photosensitization: effects, mechanism and therapeutic implications, *Clin. Cancer Res.* 12 (2006) 917–923.
- [19] Z. Zhen, W. Tang, Y.J. Chuang, T. Todd, W. Zhang, X. Lin, G. Niu, G. Liu, L. Wang, Z. Pan, et al., Tumor vasculature targeted photodynamic therapy for enhanced delivery of nanoparticles, *ACS Nano* 8 (2014) 6004–6013.
- [20] A. Wagner, U.W. Denzer, D. Neureiter, T. Kiesslich, A. Poespoeck, E.A.J. Rauws, K. Emmanuel, N. Degenhardt, U. Frick, U. Beuers, et al., Temoporfin improves efficacy of photodynamic therapy in advanced biliary tract carcinoma: a Multicenter prospective phase II study, *Hepatology* 62 (2015) 1456–1465.
- [21] L. Caesar, T.E.M. van Doeveren, I.B. Tan, A. Dilci, R.L.P. van Veen, B. Karakullukcu, The use of photodynamic therapy as adjuvant therapy to surgery in recurrent malignant Tumors of the Paranasal sinuses, *Photodiagn. Photodyn. Ther.* 12 (2015) 414–421.
- [22] M. Nitta, Y. Muragaki, T. Maruyama, H. Iseki, T. Komori, S. Ikuta, T. Saito, T. Yasuda, J. Hosono, S. Okamoto, et al., Role of photodynamic therapy using Talaporfin sodium and a semiconductor laser in patients with newly diagnosed Glioblastoma, *J. Neurosurg.* 131 (2019) 1361–1368.
- [23] T. Yano, H. Kasai, T. Horimatsu, K. Yoshimura, S. Teramukai, S. Morita, H. Tada, Y. Yamamoto, H. Kataoka, N. Kakushima, et al., A Multicenter phase II study of salvage photodynamic therapy using Talaporfin sodium (ME2906) and a diode laser (PNL6405EPG) for local failure after Chemoradiotherapy or radiotherapy for Esophageal cancer, *Oncotarget* 8 (2017) 22135–22144.
- [24] L.J. Cruz, P.J. Tacken, R. Fokkink, B. Joosten, M.C. Stuart, F. Albericio, R. Torensma, C.G. Figdor, Targeted PLGA Nano- but not microparticles specifically deliver antigen to human dendritic cells via DC-SIGN in vitro, *J. Control. Release* 144 (2010) 118–126.
- [25] L.J. Cruz, P.J. Tacken, F. Bonetto, S.I. Buschow, H.J. Croes, M. Wijers, L.J. de Vries, C.G. Figdor, Multimodal imaging of Nanovaccine carriers targeted to human dendritic cells, *Mol. Pharm.* 8 (2011) 520–531.
- [26] L.J. Cruz, P.J. Tacken, F. Rueda, J.C. Domingo, F. Albericio, C.G. Figdor, Targeting nanoparticles to dendritic cells for immunotherapy, *Methods Enzymol.* 509 (2012) 143–163.
- [27] L.J. Cruz, M.A. Stammes, I. Que, E.R. van Beek, V.T. Knol-Blankevoort, T.J.A. Snoeks, A. Chan, E.L. Kaijzel, C.W.G.M. Löwik, Effect of PLGA NP size on efficiency to target traumatic brain injury, *J. Control. Release* 223 (2016) 31–41.
- [28] F. van Leeuwen-van Zaane, P.B.A.A. van Driel, U.A. Gamm, T.J.A. Snoeks, H.S. de Bruijn, A. van der Ploeg-van den Heuvel, C.W.G.M. Löwik, H.J.C.M. Sterenberg, A. Amelink, D.J. Robinson, Microscopic analysis of the localization of two Chlorin-based photosensitizers in OSC19 Tumors in the mouse Oral cavity, *Lasers Surg. Med.* 46 (2014) 224–234.
- [29] M. Korbelik, I. Cecic, Contribution of myeloid and lymphoid host cells to the curative outcome of mouse sarcoma treatment by photodynamic therapy, *Cancer Lett.* 137 (1999) 91–98.
- [30] A. Kumari, S.K. Yadav, S.C. Yadav, Biodegradable polymeric nanoparticles based drug delivery systems, *Colloids Surf. B: Biointerfaces* 75 (2010) 1–18.
- [31] J. Khan, A. Alexander, Ajazuddin, S. Saraf, S. Saraf, Exploring the role of polymeric conjugates toward anti-cancer drug delivery: current trends and future projections, *Int. J. Pharm.* 548 (2018) 500–514.
- [32] D.A. Kuhn, D. Vanhecke, B. Michen, F. Blank, P. Gehr, A. Petri-Fink, B. Rothen-Rutishauser, Different Endocytotic uptake mechanisms for nanoparticles in epithelial cells and macrophages, *Beilstein J. Nanotechnol.* 5 (2014) 1625–1636.
- [33] H.L. Herd, K.T. Bartlett, J.A. Gustafson, L.D. McGill, H. Ghandehari, Macrophage silica nanoparticle response is phenotypically dependent, *Biomaterials* 53 (2015) 574–582.
- [34] H.H. Gustafson, D. Holt-Casper, D.W. Grainger, H. Ghandehari, Nanoparticle uptake: the phagocyte problem, *Nano Today* 10 (2015) 487–510.
- [35] G. Krosli, M. Korbelik, G.J. Dougherty, Induction of immune cell infiltration into murine SCCVII tumour by Photofrin-based photodynamic therapy, *Br. J. Cancer* 71 (1995) 549–555.
- [36] M. Korbelik, PDT-associated host response and its role in the therapy outcome, *Lasers Surg. Med.* 38 (2006) 500–508.
- [37] A. Jalili, M. Makowski, T. Switaj, D. Nowis, E. Wilczek, M. Chora, Effective Photoimmunotherapy of murine Colon carcinoma induced by the combination of photodynamic therapy and dendritic cells, *Clin. Cancer Res.* 10 (2004) 4498–4508.